ISBN: 978-3-95450-203-5 doi:10.18429/JACoW-HIAT2018-THOAA01

HIGH RESOLUTION MASS SEPARATOR DIPOLE DESIGN STUDIES FOR SPES PROJECT

C. Baltador, M. Comunian, L. Bellan, M. Cavenago, A. Galatà, L. Ferrari, A. De Lorenzi*, F.Mosio and A.Pisent

INFN-LNL, [35020] Legnaro, Italy
*Consorzio RFX,[35127] Padova, Italy

Abstract

The purposes of the SPES (Selective Production of Exotic Species) project at INFN laboratory in Legnaro (Italy) is to study nuclei close to the drip lines. Therefore, a High-Resolution Mass Separator (HRMS) must provide full separation of the ions with a resolution 1/20000, to be sensible to the proton-neutron mass difference in the fission products. SPES HRMS consists of: two 90° magnet dipoles, one electrostatic multipole in between them, six electrostatic quadrupoles, two electrostatic hexapoles and two electrostatic triplets before and after the slits on the object and image point. All these components will be installed on a high voltage platform with a maximum operating voltage of -240 kV. Before entering the HRMS, a 40 keV energy beam go through an RFQ Cooler, designed to have an output energy spread of 1 eV. Mass separation within target resolution is the most critical part: dipoles must provide a magnetic field homogeneity of 4 10^{-5} throughout beam occupancy (half magnet pole surface), at a field intensity of 0.562 T for the reference ion 132 Sn. Therefore, a very accurate dipole design is mandatory. This contribute will show the studies which lead to a possible dipole design.

INTRODUCTION

The Selective Production of Exotic Species (SPES) project at INFN-LNL Legnaro, Italy is a radioactive ion beam (RIB) facility [1,2]. Many field of interests will characterize its experimental life, ranging from basic research in nuclear physics and astrophysics to interdisciplinary applications, like production of radionuclides of medical interest and the generation of neutrons for material studies, nuclear technologies and medicine. SPES RIB production is based on the ISOL method with an UCx Direct Target able to sustain a power of 10 kW. The primary proton beam is delivered by a high current Cyclotron accelerator, with energy 35-70 MeV and a beam current of 0.2-0.5 mA. Neutron-rich radioactive ions will be produced by proton induced Uranium fission in the UCx target at an expected fission rate in the order of 10^{13} fissions per second. The exotic isotopes will be re-accelerated by the ALPI superconducting LINAC at energies of 10A MeV and higher, for masses in the region A=130 amu at expected rate on the secondary target of 10^7 – 10^9 pps.

In the framework of the SPES project, the High-Resolution Mass Spectrometer (HRMS) must provide high purification of the ^{132}Sn ion beam and > 95% transmission. The design goal is to achieve a mass resolving power $\Delta m/m = 1/20000$.

HRMS LAYOUT

The design choices made for the HRMS are common from the medium mass separator (MRMS) of SPES [3], which is now under installation and will be used as a test stand for the HRMS. Similar optics layout is used in recent projects [4,5,6], with different choice of parameters.

The HRMS general layout, which is perfectly symmetric with respect to the central axis, is presented in Fig. 1.

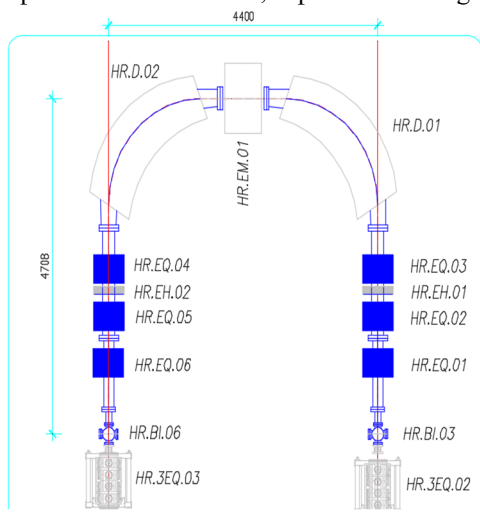

Figure 1: HRMS layout on high voltage platform.

HRMS will be installed on a High Voltage platform (represented by the light blue line) with a maximum operating voltage of -240 kV. The beam, which is extracted from the source with 40 keV energy, enters HRMS from the right-hand side branch of the device. The object and image slits (HR.BI.03-6) delimit separator entrance and exit.

More in details, following the beam path, an accelerating column (HR.AT.01) gradually accelerates the beam to accommodate its energy for the HV platform and then it will pass through the following components:

- an electrostatic triplet (HR.3EQ.02);
- two electrostatic quadrupoles (HR.EQ.01-2);
- one electrostatic hexapole (HR.EH.01-2);
- a single electrostatic quadrupoles (HR.EQ.03);
- a magnetic dipole (HR.D.01-2), H-shaped with bending angle $\varphi = 90°$;
- one electrostatic multipole (HR.EM.01);

Content from this work may be used under the terms of the CC BY 3.0 licence (© 2018). Any distribution of this work must maintain attribution to the author(s), title of the work, publisher, and DOI.

ISBN: 978-3-95450-203-5 doi:10.18429/JACoW-HIAT2018-THOAA01

After the multipole, the beam will pass through the same array, but with inversed order.

From the optical point of view, the spacing between the elements is set to achieve unit magnification imaging from slit to slit in the horizontal plane. Hexapoles are added to provide dynamics correction aberration: in a separator the horizontal size of the beam is large in the dipoles so that geometrics aberrations occur. The triplet is needed to create a waist into the object point of the separator. All the components, excluding the dipoles, are electrostatic to avoid mass dependences outside the dipoles, for a given energy. Table 1 summarizes the specifications of the various components.

Table 1: HRMS Components Specifications

Element	Nom. Value	Units / Note
HR.3EQ.02/03	-7 / +6 / -7	kV / triplet
HR.BI.03/06	1.1	mm/object-image
HR.EQ.01/06	-9.6	kV
HR.EQ.02/05	+4	kV
HR.EH.01/02	< 1	kV / hexapole
HR.EQ.03/04	-6	kV
HR.D.01/02	0.5623	T
HR.EM.01	< 1	kV /multipole

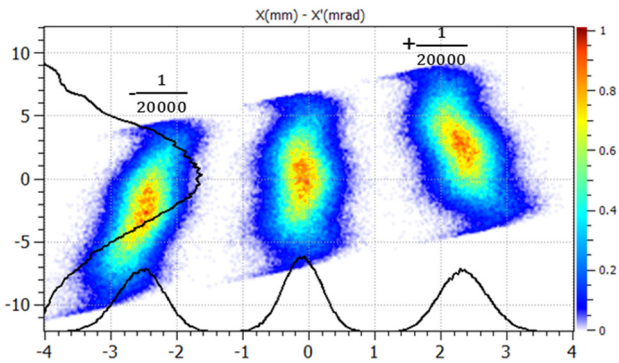

Figure 2: Emittances of three resolved isobars at image slit as from beam optics simulations (Tracewin).

HIGH RESOLUTION ISSUES

Mass resolution relates directly with the displacement Δx of the beam at the image point with respect to the position at the object slit through the relation:

$$\Delta x = D\frac{dm}{m} \qquad (1)$$

where D is the dispersion of the separator. In general, the larger Δx the lower the horizontal overlap of the separated isobars at the image point. Large dispersion is therefore needed: in HRMS case 100 m dispersion is expected, leading to 2.5 mm isobar separation at image slit, provided the 1/20000 mass resolution (see Fig. 2).

However, many issues can degrade the resolutive power of a separator. In this contribution only general overview is presented, while a deep study about sources of performance degradation for HRMS is presented in [7].

Magnetic mass separators, like HRMS, discriminates momentum, since deflection of charged particles under an external vertical magnetic field, is described by the magnetic rigidity relation:

$$B\rho = \frac{p}{q} \qquad (2)$$

By applying the logarithm derivatives to $p^2 = 2mE$ (m the mass and $E = qV$ the energy of the particle), one has:

$$2\frac{dp}{p} = \frac{dm}{m} + \frac{dE}{E} \qquad (3)$$

This gives the important information that energy variation can have the same effect as a mass variation. Hence, the energy spread of the beam must be in of the same order mass resolution, otherwise HRMS performances would be affected. This immediately translates in terms of voltage stability of the high voltage platform to be in the range of less than 1V for a nominal beam of 260 keV.

Beam emittance also needs to be as small as possible. Emittance ε and mass resolution relates through the relation:

$$\frac{dm}{m} = \frac{2\varepsilon}{D\,x'}, \qquad (4)$$

being x' the beam divergence. Equation (4) shows that a beam featuring small emittance is mandatory for achieving the needed purification level. An RFQ Cooler (currently under development by LPC [8]) is prescribed to be placed before HRMS entrance to reduce energy spread and emittance: its design goals are indeed an output energy spread >±1eV and transverse emittance reduction by a factor 10. From the combined action of C-RFQ and the acceleration provided by the HV platform a 3.2 mm mrad geometric emittance is expected at object slit.

Anyway, the most critical role to satisfy the requirements for a mass separation resolution of 1/20000 is played by the two dipoles, in terms of mechanical design. This can be easily understood, since the wanted resolution implies a very high magnetic field homogeneity within the poles. From (2), since $v = \sqrt{2mV/q}$, by logarithm derivations one gets:

$$\frac{dB}{B} = \frac{1}{2}\frac{dm}{m} \qquad (5)$$

Hence, field deviation from the reference value must lie within a range of the same order of magnitude of the mass separation that has to be resolved. i.e. 5 10^{-5}. Otherwise a field variation would act as a mass variation, in the same fashion as discussed before for the energy spread.

DIPOLE DESIGN

Designing a suitable dipole capable to achieve the field homogeneity needed to preserve the 1/20000 mass

Content from this work may be used under the terms of the CC BY 3.0 licence (© 2018). Any distribution of this work must maintain attribution to the author(s), title of the work, publisher, and DOI.

ISBN: 978-3-95450-203-5 doi:10.18429/JACoW-HIAT2018-THOAA01

Content from this work may be used under the terms of the CC BY 3.0 licence (© 2018). Any distribution of this work must maintain attribution to the author(s), title of the work, publisher, and DOI.

resolution is therefore mandatory for the HRMS. Table 2 summarizes main beam reference parameters.

HRMS features two H-shaped dipoles with bending angle $\varphi = 90°$. The following relation directly relates the curvature radius to the dispersion generated by a dipole:

$$D = \rho(1 - \cos\varphi) \qquad (6)$$

When the bending angle is $\varphi = 90°$ than $D = \rho$. Therefore, two identical dipoles, like in our case, would double the dispersion. Of course, one single 180° dipole would act in the same fashion, but this configuration allows for the installation of the electrostatic multipole for high order aberration corrections [9]. From equation (1), we know that large dispersions values are beneficial for the mass resolution. Unfortunately, practical limitations to the overall HRMS size is due to the small space available on site, for the platform and the overall services around it. The maximum possible curvature radius for the dipoles is $\rho = 1500$ mm.

Table 2: Beam Reference Parameters

Geometric Emittance	3.2	4σ mm*mrad
Ion Mass (q=1)	132	amu
Beam Energy	260	KeV
RMS Energy Spread	1	eV
RMS Spot size at image	0.3	mm
Maximum X range	500	mm

The reference vertical magnetic field inside the dipoles is then derived from the rigidity relation (2) as $B_{y-ref} = 0.562\ T$.

The entrance and exit edges of the magnetic dipoles are angled ($\alpha = 27°, 16'$) with respect to the beam trajectory to provide vertical focusing. Edges also feature circular curvatures to correct hexapole aberrations deriving from second order components of the dipole field:

$$r_{edge} = \frac{B_{y-ref}}{2C_{hexapole}}(\sec\alpha)^3 \qquad (7)$$

where $C_{hexapole} = 0.163\ T/m$ is the hexapole term coefficient, given by Tracewin [10] simulations.

From beam optical simulations done with Tracewin, info on beam horizontal and vertical extensions can be obtained (see bottom part of Fig. 3. These information are needed for pole gap and length sizing. The electrostatic components of the HRMS are configured to produce a very narrow beam at the dipole entrance, but despite a 40 mm pole gap of can be enough as vertical acceptance, helping also for power saving, a too complex vacuum chamber installation pushed for a 60 mm gap.

Turing to the pole length, the choice of an initial 900 mm was made with the rule of thumb to almost double the horizontal beam extension of 500 mm (see upper part of Fig. 3). It was then possible to optimize this value to 860 mm. In more details the density profiles given by Tracewin state that the 68% of the beam lies within ± 115 mm, the 90% within ± 220 mm and the 99% within ± 250 mm, with respect to the optical axis.

The size of the coil cross section, chosen on power saving considerations, and the magnetization level of the iron in working condition, define the return yoke size. It is important to try to keep the magnet working as much as possible, in the linear range of the B-H curve: in our case, we have considered XC06 iron and the magnetization level limit of 1.6 T, which was a good compromise between magnetization level and magnet weight. A summary of the main dipole parameters are listed in Table 3.

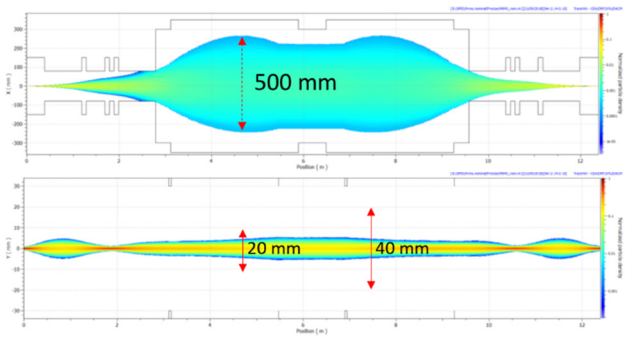

Figure 3: Beam density on horizontal (top) and vertical (bottom) planes, from object slit to image slit (Tracewin).

Table 3: Dipole Parameters

Radius	1500	mm
Bending Angle	90	Deg
Vertical Gap (wrt centre)	± 30	mm
Pole length (wrt centre)	± 430	mm
Nominal Magnetic Field	0.562	T
Edge Angle	27.16	Deg
Edge Hexapole radius	2220	mm
Iron max. magn. level	1.6	T
Coil current density	4.2	A/mm^2
Power	28	kW

FIELD OPTIMIZATION

As discussed before, the most critical aspect for achieving the 1/20000 resolution for the HRMS is the field homogeneity in between the two poles. The challenge arise not only by the homogeneity level 5 10^{-5}, but especially because this goal has to be achieved throughout all the area where the beam is intended to pass inside the dipole that is very large, since the high dispersion inside the dipole (upper part of Fig. 3). The idea is that the magnet must behave like an ideal infinite, hard-edge dipole.

A possible approach that can be followed for the optimization process is to optimize the dipole cross section shape at first, achieving the desired homogeneity along the transverse direction with respect to the optical axis, with 2D simulations. The optimized cross section can then be transposed to the third dimension, where a second optimization process is needed to consider the asymmetry introduced by the dipole-bending angle.

The observable throughout all the process is the field flatness, defined as:

ISBN: 978-3-95450-203-5 doi:10.18429/JACoW-HIAT2018-THOAA01

$$\left(\frac{B_y(s)}{B_{y-ref}}\right) - 1 = 0 \pm 4\,10^{-5} \qquad (8)$$

where s is the pole length x-position for the 2D simulations and the longitudinal angular position of the dipole in the 3D simulations. With this definition for the flatness, we are looking for a profile that is zero within the $4\,10^{-5}$ range.

The following design studies were carried out with the TOSCA package of the commercial fem software OPERA-3D [11].

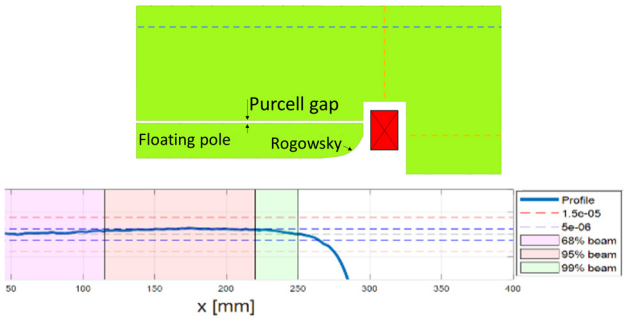

Figure 4: Cross sectional view of ¼ dipole (top) and Flatness profile (bottom).

2D Optimization

With 2D simulations, it is possible to investigate the best design solution for the field flatness in the transverse direction with respect to the optical axis. Many solutions were investigated. In the end, the best result was obtained with the Purcell-cell design, in combination with the Rogowsky shaped pole edge.

The Purcell-cell design consists in a fully magnetically detached pole from the rest of the yoke. We can address to the detached pole as the 'floating pole', while to the gap in between as 'Purcell gap' (see upper part of Fig. 4). The Rogowsky edge profile is a curve given by the following equation:

$$y_{Rog} = G\left(\frac{1}{2} + \frac{1}{\pi}e^{\left(\frac{\pi x}{G}-1\right)}\right), \qquad (9)$$

where y_{Rog} is the y position at which the Rogowsky curve has to stop and G is the full dipole gap.

With a correct choice of Purcell gap vertical position and y_{Rog}, a flatness profile within $5\,10^{-6}$ was even achievable. The lower part of Fig. 4 show the flatness profile, as defined by equation (8), in function of the pole length. The vertical axis is limited to the reference flatness goal of $4\,10^{-5}$, while dashed lines are reference flatness values. Lastly, horizontal beam density information are given by the coloured areas: the 68% of the beami is enclosed by the pink area, the 99% by the red and the 99% by the green one.

3D Optimization

Moving to the third dimension the bending angle of the dipole introduces an asymmetry that cannot be considered in the two 2D cross section. This asymmetry generates a field hot-spot in the dipole 'elbow'. This is show in the B_y map *a*) of Fig. 5. This field map corresponds to the simple extrusion of the 2D cross section presented in the upper part of Fig. 4, to which hexapole curvatures to the entrance and exit faces was added only. Note that the colour scale in Fig. 5 ranges within $\pm 10^{-4}$ with respect to B_{y-ref}.

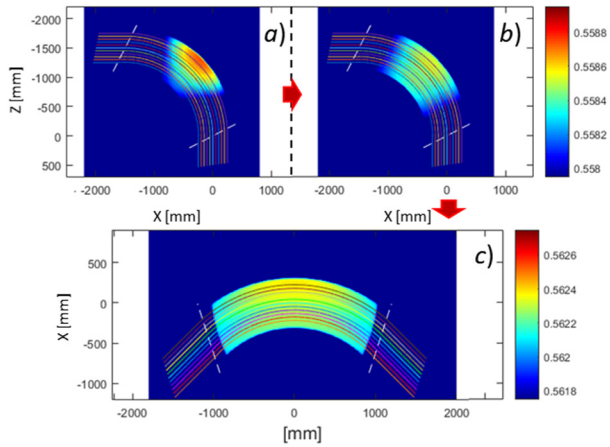

Figure 5: Field homogeneity rough optimization. Field maps inside the dipole after: *a*) simple extrusion of 2D cross section; *b*) magnetic flux balance; *c*) Rogowsky profile extended to the entrance and exit edges.

Therefore, for flatness optimization, the asymmetry has to be counteracted. Since it consists in a different amount of iron between the internal and external curvature of the dipole, a good way to proceed is to balance the magnetic fluxes in the internal and external return yokes. The lack of iron in the internal curvature causes the increase of the magnetization level and consequently of the local relative permeability of the iron: this acts like a bottleneck for the magnetic flux. To restore the flux balance, the internal and external return yoke horizontal and vertical surfaces should be equalized, respectively. The two surfaces are highlighted with yellow dashed lines in the upper part of Fig. 4. This equalization can be done by increasing the amount of iron in the internal curvature for the horizontal surface, while cutting away iron as highlighted by the blue dashed line in Fig. 4, on the external part of the yoke for the vertical one. The latter step causes the magnet top and bottom external surfaces to be not flat as usual. This is also beneficial for dipole weight.

The result of this flux balance can be seen in the field map *b*) of Fig. 5. In Fig. 5 the field uniformity is now enhanced in the dipole centre, but there still something missing at the entrance and exit of the dipole.

It makes sense, then, to extend the Rogowsky shape also to the entrance and exit faces of the floating pole. Until now, it was applied to the floating pole lateral edges only, as consequence of the extrusion of the 2D cross section. The consequences of this step are shown in the field map *c*) of Fig. 5, while Fig. 6 shows the model of the dipole, obtained so far.

Content from this work may be used under the terms of the CC BY 3.0 licence (© 2018). Any distribution of this work must maintain attribution to the author(s), title of the work, publisher, and DOI.

ISBN: 978-3-95450-203-5 doi:10.18429/JACoW-HIAT2018-THOAA01

Content from this work may be used under the terms of the CC BY 3.0 licence (© 2018). Any distribution of this work must maintain attribution to the author(s), title of the work, publisher, and DOI.

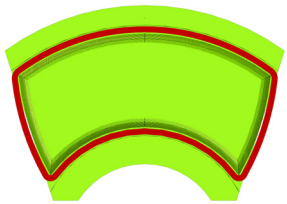

Figure 6: OPERA model of the dipole: view of the pole face.

Let refer to this last step as '*opt-0*'. It is now possible to look at the field flatness again but considering a flatness profile along the beam propagation direction, instead of transverse direction, like in the 2D case. In this way, it is possible to have longitudinal information about the field homogeneity. The transversal information can be obtained this time by considering not only the flatness profile at the optical axis ($\rho = 1500\ mm$) but also at different curvature radius. In the following plots, flatness profiles in 50 mm steps far away from the optical axis are reported, so that the entire beam horizontal extension (99% of the beam lie within ± 250 mm wrt to ρ) is observed. The trajectories of these profiles are visible in the field maps of Fig. 5. In the flatness profiles in Fig. 7 the vertical axis gives information about the homogeneity level, the horizontal axis now gives longitudinal information, while the different lines give transversal information.

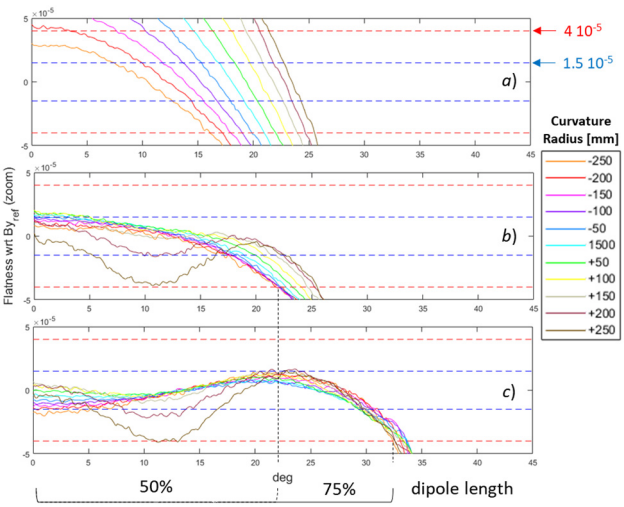

Figure 7: Flatness profiles at different curvature radius: *a*) opt-0; *b*) opt-1; *c*) opt-3.

The upper plot *a*) of Fig. 7 refers to the flatness of the *opt-0* step. It is clear that further optimization is still needed, since a vertical field hot-spot at the dipole 'elbow' is still present even if strongly weakened than before.

By applying a net cut to the floating pole 'elbow' only, it is possible to damp the hot-spot with high accuracy (*opt-1* step). Flatness is now within the reference range (red dashed line), enclosing the 99% of the beam for the 50% of the dipole length (Fig. 7b).

A further extension of the flatness along the longitudinal direction is possible by introducing some field reinforcement inside the Purcell-gap, at the entrance and exit faces (*opt-2* step). A correct sizing of the reinforcements can extend field flatness up to the 75% of the pole length, as shown by *c*) plot of Fig. 7.

Lastly, fringe field effect must be taken into account as well. Fringe field causes the magnetic length of the dipole to be different with respect to the hard-edge model, given by $L_{hard-edge} = \frac{\pi}{2}\rho$. The effective magnetic length can be obtained with:

$$L_{eff} = \frac{\int_{-\infty}^{\infty} B_y(s)ds}{B_y(0)} \qquad (10)$$

, where s is the curvilinear coordinate along the dipole length. To have $L_{hard-edge} = L_{eff}$ condition, field clamps can be added to the entrance and exit dipole faces (see lhs of Fig. 8). By placing the clamp at the proper distance from the pole face, it is possible to cancel the difference between the two lengths (see rhs of Fig. 8).

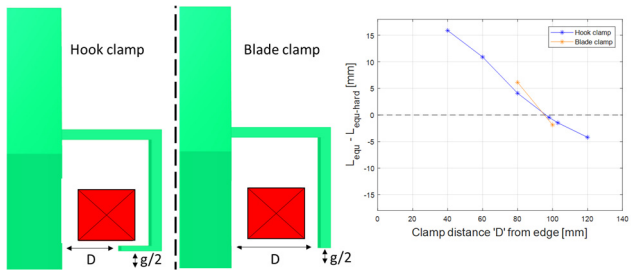

Figure 8: Two possible field clamp configurations (left), both capable to cancel the fringe field effect (right).

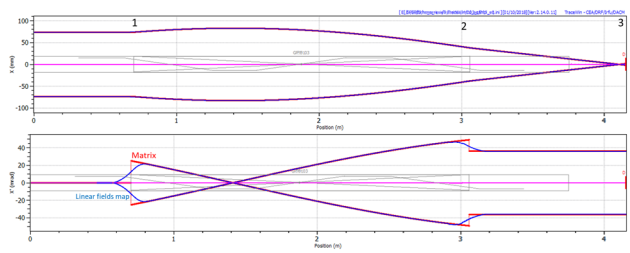

Figure 9: Beam optics inside dipole simulations with Tracewin: comparison between theoretical hard-edge matrix model (red line) and field map (blue line) from dipole final design with OPERA simulation.

It is now possible to check dipole field, obtained from this study, with beam optics simulations. Figure 9 shows a perfect agreement between a theoretical, matrix-modelled, hard-edge dipole (doubled checked with COSY-infinity [2]) and the same simulation done using the field map obtained with OPERA simulations.

CONCLUSIONS

The design studies performed with OPERA simulations demonstrate that a dipole with a field flatness suitable for a separator with a resolution of 1/20000 is feasible. Mechanical and electrical tolerances are currently under investigation and preliminary studies are giving encouraging results with very strict tolerances, but anyhow reasonable. Since the engineering of the design here presented was not done yet, this is can be considered a feasibility study only.

ISBN: 978-3-95450-203-5 doi:10.18429/JACoW-HIAT2018-THOAA01

REFERENCES

[1] G. Bisoffi, *et al.,* "Progress in the realization and commissioning of the exotic beam facility SPES at INFN-LNL", 2018 J. Phys.: Conf. Ser. 1067 052017.

[2] M. Comunian, *et. al.,* "Status of the SPES Exotic Beam Facility", presented at the 14th Int. Conf. on Heavy Ion Accelerator Technology (HIAT'18), Lanzhou, China, Oct. 2018, paper MOYAA02, this conference.

[3] A. Galata, *et al.,* "ADIGE: the radioactive ion beam injector of the SPES project", in *Proc. 8th Int. Particle Accelerator Conf. (IPAC'17)*, Copenhagen, Denmark, May 2017, pp. 2281, doi:10.18429/JACoW -IPAC2017-TUPVA087

[4] C.N. Davids, *et al.,* "A compact high resolution isobar separator for the CARIBU project" in *Proc. PAC'09*, Vancouver, Canada, May 2009, paper FR5REP116, pp. 5050.

[5] J.A. Maloney, *et al.,* "New design studies for TRIUMF's ARIEL High Resolution Separator", Nucl. Instrum. and Methods Phys Res. Section B, 376 (2016) https://doi.org/10.1016/j.nimb.2015.11.023.

[6] T. Kurtukian-Nieto, *et al.,* "SPIRAL2/DESIR high resolution mass separator" Nulc. Instrum. and Methods. Phys Res. Section B, 317 (2013)

[7] M. Comunian, *et al.,* "Design of high resolution mass spectrometer for SPES", in *Proc. IPAC'18*, Vancouver, Canada, Apr.-May 2018, pp. 3252, doi:10.18429/JACoW-IPAC2018-THPAK021

[8] A. Nieminen, *et al.,* "Beam Cooler for Low-Energy R dioactive Ions", Nuclear Instruments and Methods in Physics Research A 469, ELSEVIER, August 2001, p. 244-253; http://www.elsevier.org

[9] L. Bellan, INFN-LNL annual Report 241 (2015) ISSN 1828-8561;

[10] D. Utriot and N. Pichoff, "TraceWin", CEA Saclay, website: http://irfu.cea.fr/Sacm/logiciels/index3.php.

[11] https://operafea.com

Content from this work may be used under the terms of the CC BY 3.0 licence (© 2018). Any distribution of this work must maintain attribution to the author(s), title of the work, publisher, and DOI.